Mechanics of granular and polycrystalline solids

Micromechanical modeling of the elasto-viscoplastic behavior of granite

Tao Zeng [a,b], Jian-Fu Shao [a,b,*], Wei-Ya Xu [a]

[a] *Hohai University, Nanjing 210098, China*
[b] *Laboratoire de mécanique de Lille, UMR 8107 CNRS, cité scientifique, 59655 Villeneuve-d'Ascq cedex, France*

A B S T R A C T

We present in this paper a micromechanics-based elasto-viscoplastic approach for modeling the time-dependent deformation of granite. Inspired by the polycrystalline theory of metallic materials, the sliding behavior in an individual grain is regarded as the sole source of plastic deformation, which is characterized by a Mohr–Coulomb-type yield criterion and a non-associated plastic potential. The micro–macro transition is realized within the framework of Hill's self-consistent approach. The performance of the proposed model is evaluated by several case studies and by reproducing experimental data.

© 2015 Académie des sciences. Published by Elsevier Masson SAS. All rights reserved.

1. Introduction

The frictional sliding of weakness planes (cracks and interfaces) inside the granite is considered as the origin of inelastic deformation [1,2]. When granite is used in some long-term facilities, e.g., underground cavities and slopes or storage of nuclear wastes, special attentions should be paid to its time-dependent deformation.

From a microscopic point of view, granite is an agglomerate of individual grains (also called crystals). The micromechanical models which regard the weakness planes as the homogeneities embedded in an intact matrix cannot appropriately represent its morphology [2,3]. Therefore, the well-developed polycrystalline model of metallic materials is adopted to characterize such kind of granular composite.

To make the model presentation clearer, some assumptions are firstly made: granite is a monomineralic geological polycrystal, since quartz is usually the dominant constituent; grains are randomly distributed and their crystal structure is fcc (granite really possesses a trigonal structure; to enable the deformation study, however, a higher crystal symmetry could be used by adding a center of symmetry [4]); the behavior of the weakness planes is similar to that of the crystallographic planes in FCC, e.g., sliding along predefined directions on certain crystallographic planes is the sole source of inelastic deformation.

The viscoplastic constitutive models for polycrystals have been well established ([5,6], just to mention some typical studies). Due to the typical features of geomaterials, however, the developed model is different from the typical ones in two aspects. Firstly, the non-smooth convex elastic domain is retained. As for geomaterials, the elastic and inelastic deformations have almost the same magnitude and therefore the former is not negligible. The existence of the elastic domain will result in numerical difficulties since the clear distinction between active and non-active slip systems must be made. A multi-level

---

* Corresponding author at: LML, UMR CNRS 8107, University of Lille, 59655 Villeneuve d'Ascq cedex, France. Tel.: +33 320434626.
  E-mail address: jian-fu.shao@polytech-lille1.fr (J.-F. Shao).
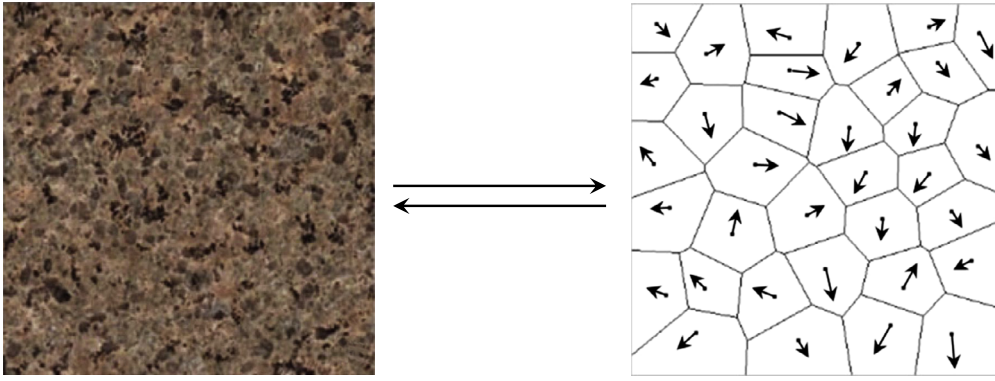
Fig. 1. (Color online.) Typical photograph of a grained granite [7] and numerical model representation. Black arrows indicate grain orientations.

iteration procedure is designed to determine the actually active slip systems when the stress state locates at these convexities. Secondly, a Mohr–Coulomb-type yield criterion and a non-associated plastic potential are introduced to reflect the characteristics of pressure sensitivity and dilation due to plastic flow.

The present paper is organized as follows: an extended self-consistent model is established at first. Then a Mohr–Coulomb-type yield criterion and a non-associated plastic potential as well as the effects of the parameters related to time-dependent deformation are presented in detail. Finally, the performance of the proposed model is evaluated by comparing the predicted results with the experimental data.

The following tensor conventions and operations are employed throughout this paper: first-order tensor $\underline{a}$; second-order tensor $\underline{\underline{a}}$; fourth-order tensor $\mathbb{A}$; double-contraction $\underline{\underline{a}} : \underline{\underline{b}} = a_{ij}b_{ij}$, $\mathbb{A} : \underline{\underline{b}} = A_{ijkl}b_{kl}$, $\mathbb{A} : \mathbb{B} = A_{ijkl}B_{klmn}$; dyadic products $\underline{a} \otimes \underline{b} = a_i b_j$.

2. Macroscopic response of granite by a self-consistent approach

A typical photograph of grained granite and the corresponding numerical representation (REV, Representative Element Volume) are given in Fig. 1. Taking its morphology into account, a self-consistent approach is necessary to obtain the macroscopic response.

2.1. Hill's incremental approach and its limitation for the elasto-viscoplastic problem

Based on the pioneering work of Hershey on elastic polycrystals [8], Hill proposed an incremental approach to approximate the properties of an elasto-plastic polycrystal [9]. He assumed that, regardless of scales, there exits a one-to-one linear relationship between strain and stress increments, namely:

$$\dot{\underline{\underline{\sigma}}}^g = \mathbb{L}^g : \dot{\underline{\underline{\varepsilon}}}^g \tag{1}$$

$$\dot{\underline{\underline{\Sigma}}} = \mathbb{L} : \dot{\underline{\underline{E}}} \tag{2}$$

The superscript g represents the grain. $\dot{\underline{\underline{\sigma}}}^g$ and $\dot{\underline{\underline{\varepsilon}}}^g$ are the stress rate and the strain rate in a single grain. $\dot{\underline{\underline{\Sigma}}}$ and $\dot{\underline{\underline{E}}}$ are the macroscopic stress rate and strain rate associated with an homogeneous equivalent medium (HEM). The HEM is an imaginary medium, which plays the same role as the matrix for intact materials in micromechanics. $\mathbb{L}^g$ and $\mathbb{L}$ represent the instantaneous moduli of grain and HEM, respectively. In the following derivations, only the superscript g on $\mathbb{L}$ and $\mathbb{A}$ (which will be referred to later) are preserved, just to simplify the labeling.

The deviations of strain and stress in any grain and HEM can be linked through a so-called 'overall constraint' tensor $\mathbb{L}^\star$:

$$\dot{\underline{\underline{\sigma}}} - \dot{\underline{\underline{\Sigma}}} = -\mathbb{L}^\star : (\dot{\underline{\underline{\varepsilon}}} - \dot{\underline{\underline{E}}}) \tag{3}$$

where

$$\mathbb{L}^\star = \mathbb{L} : (\mathbb{S}^{-1} - \mathbb{I})$$

$\mathbb{I}$ is a fourth-order unit tensor. $\mathbb{S}$ is the well-known Eshelby tensor, which is the function of $\mathbb{L}$ in this paper. For more complicated cases, refer to [6].

Substituting (1) and (2) into (3) and after some algebra operations, the strains in grain and HEM could be related through a concentration tensor $\mathbb{A}^g$:

$$\dot{\underline{\underline{\varepsilon}}} = \mathbb{A}^g : \dot{\underline{\underline{E}}} \tag{4}$$

where

$$\mathbb{A}^g = \left(\mathbb{L}^\star + \mathbb{L}^g\right)^{-1}\left(\mathbb{L}^\star + \mathbb{L}\right)$$

Making use of (1), (2) and (4) and taking into account the micro–macro transition $\langle \underline{\dot{\sigma}} \rangle = \underline{\dot{\Sigma}}$, we finally obtain the following self-consistent equation:

$$\mathbb{L} = \left\langle \mathbb{L}^g : \mathbb{A}^g \right\rangle \tag{5}$$

where $\langle \cdot \rangle$ denotes volume average. For polycrystal model, it also represents an average over all grain orientations, which can be numerically calculated as follows:

$$\langle \cdot \rangle = \sum_{n=1}^{N_g} f_g \langle \cdot \rangle \tag{6}$$

N_g is the number of grains that represent the polycrystal. f_g is the volume fraction of each grain. For the polycrystal considered here (with grains randomly distributed), $f_g = 1/N_g$.

Nevertheless, all above derivations are based on the foremost assumption that the one-to-one stress–strain relationship exists. Unfortunately, this is not the case for the viscoplastic problem. Although the microscopic consistent algorithmic tangent moduli could be derived (also the macroscopic one by solving (5)), the macroscopic stress–strain response still cannot be deduced from (2).

2.2. Extension of Hill's incremental approach

To obtain macroscopic stress–strain response, we rewrite the constitutive equation (2) as:

$$\underline{\dot{\Sigma}} = \mathbb{C}^{\mathrm{hom}} : \left(\underline{\dot{E}} - \underline{\dot{E}}^{\mathrm{vp}}\right) \tag{7}$$

where $\mathbb{C}^{\mathrm{hom}}$ is the homogenized elastic moduli of HEM. In this paper, only the isotropic elasticity is considered. Therefore, $\mathbb{C}^{\mathrm{hom}} = \mathbb{C}^g = \mathbb{C}$.

From (7), it is straightforward to infer that as long as $\underline{\dot{\varepsilon}}^{\mathrm{vp}}$ is available, the macroscopic stress could be immediately calculated with the help of (6):

$$\underline{\dot{E}}^{\mathrm{vp}} = \left\langle \underline{\dot{\varepsilon}}^{\mathrm{vp}} \right\rangle \tag{8}$$

The whole procedure is outlined as follows: at a given time t, all solution-dependent variables have been determined. Then, a new macroscopic strain increment ΔE is prescribed (only the strain-driven case is considered, since it is convenient to be implemented into FEM software). Our goal is to determine $\Delta \underline{E}^{\mathrm{vp}}$ at $t + \Delta t$ (or precisely $\Delta \underline{\varepsilon}^{\mathrm{vp}}$ of each grain at $t + \Delta t$). The whole problem is solved by means of two nested iterative procedures. A tentative guess is made for the strain increment of each grain according to (4). For the first iteration, the assumption that $\Delta \underline{\varepsilon} = \Delta E$ is made. The $\mathbb{L}^{\mathrm{alg}}$ derived in Appendix A is then calculated. For the innermost loop, a new estimation of $\mathbb{L}$ is calculated iteratively with (6) until two estimations between successive iterations are within a certain tolerance. With the most recently estimated $\mathbb{L}$ and $\mathbb{L}^{\mathrm{alg}}$, the strain increment belonging to any grain is recalculated with (4) (with $\mathbb{L}^g$ replaced by $\mathbb{L}^{\mathrm{alg}}$). The outermost loop repeats until a certain tolerance between two successive strain increments has arrived. Once two convergence values are simultaneously satisfied, the macroscopic stress increment is updated with (7) and (8).

3. Modified constitutive relations of the grain

In this section, the modified constitutive equations of the grain are briefly presented. Two operating levels: mesoscopic (grain) and microscopic (crystallographic plane); and three steps: stress projection, viscoplastic strain determination and accumulation, are concerned.

Under the assumption of infinitesimal deformation, strain satisfies the principal of superposition. For a non-linear constitutive model, it is preferable to write it in rate form as:

$$\underline{\dot{\varepsilon}} = \underline{\dot{\varepsilon}}^{\mathrm{e}} + \underline{\dot{\varepsilon}}^{\mathrm{vp}} \tag{9}$$

For the mesoscopic level, only elastically isotropic constitutive relations are taken into account. In any grain, the stress–strain response is related by Hooke's Law:

$$\underline{\dot{\sigma}} = \mathbb{C} : \underline{\dot{\varepsilon}}^{\mathrm{e}} = \mathbb{C} : \left(\underline{\dot{\varepsilon}} - \underline{\dot{\varepsilon}}^{\mathrm{vp}}\right) \tag{10}$$

$\mathbb{C}$ is the fourth-order elastic stiffness tensor of grain, which can be characterized by two elastic constants: bulk modulus k and shear modulus μ:

Table 1
Miller indices for twelve slip systems.

No.	$\underline{n}$	$\underline{s}$	No.	$\underline{n}$	$\underline{s}$	No.	$\underline{n}$	$\underline{s}$	No.	$\underline{n}$	$\underline{s}$
1	$(1\,1\,1)$	$[0\,\bar{1}\,1]$	4	$(\bar{1}\,\bar{1}\,1)$	$[0\,1\,1]$	7	$(\bar{1}\,1\,1)$	$[0\,\bar{1}\,1]$	10	$(1\,\bar{1}\,1)$	$[0\,1\,1]$
2	$(1\,1\,1)$	$[1\,0\,\bar{1}]$	5	$(\bar{1}\,\bar{1}\,1)$	$[\bar{1}\,0\,\bar{1}]$	8	$(\bar{1}\,1\,1)$	$[1\,0\,\bar{1}]$	11	$(1\,\bar{1}\,1)$	$[1\,0\,\bar{1}]$
3	$(1\,1\,1)$	$[\bar{1}\,1\,0]$	6	$(\bar{1}\,\bar{1}\,1)$	$[1\,\bar{1}\,0]$	9	$(\bar{1}\,1\,1)$	$[1\,1\,0]$	12	$(1\,\bar{1}\,1)$	$[\bar{1}\,\bar{1}\,0]$

$$\mathbb{C} = 3k\mathbb{K} + 2\mu\mathbb{J} \tag{11}$$

$\mathbb{K}$ and $\mathbb{J}$ are two fourth-order isotropic tensors allowing extracting spherical and deviatoric parts of any second-order symmetric tensor.

The assumption has been made that the sliding of the weakness planes in individual grain (along certain directions on specified crystallographic planes) is the sole source of non-linear deformation. Schmid's Law considers that the sliding behavior is pressure independent and volume conserved. However, this is not true for geomaterials. In this paper, a Mohr–Coulomb type yield criterion f and a non-associated plastic potential F are introduced to describe the sliding behavior of each slip system:

$$f^{\alpha}\big(\underline{\underline{\sigma}}, R^{\alpha}\big) = \underline{\underline{\sigma}} : \underline{\underline{P}}^{\alpha} + \mu_f H\big(-\sigma_n^{\alpha}\big)\underline{\underline{\sigma}} : \underline{\underline{N}}^{\alpha} - \big(\tau_c + R^{\alpha}\big) \tag{12}$$

$$F^{\alpha}\big(\underline{\underline{\sigma}}, R^{\alpha}\big) = \underline{\underline{\sigma}} : \underline{\underline{P}}^{\alpha} + v_F H\big(-\sigma_n^{\alpha}\big)\underline{\underline{\sigma}} : \underline{\underline{N}}^{\alpha} - \big(R^{\alpha} - bq^{\alpha}R^{\alpha}\big) \tag{13}$$

with

$$\underline{\underline{P}}^{\alpha} = \frac{1}{2}\big(\underline{s}^{\alpha} \otimes \underline{n}^{\alpha} + \underline{n}^{\alpha} \otimes \underline{s}^{\alpha}\big) \qquad \underline{\underline{N}}^{\alpha} = \underline{n}^{\alpha} \otimes \underline{n}^{\alpha} \quad \text{and} \quad \sigma_n^{\alpha} = \underline{\underline{\sigma}} : \underline{\underline{N}}^{\alpha}$$

The index $\alpha \in \{1, 2, \ldots, m\}$. m is the maximum number of octahedral systems in the grain ($m = 12$ for grain with FCC crystal structure). $\underline{n}^{\alpha}$ and $\underline{s}^{\alpha}$ are two orthogonal vectors defining the normal of crystallographic plane and the slip direction. $\underline{\underline{P}}^{\alpha}$ and $\underline{\underline{N}}^{\alpha}$ are the shear stress and the normal stress projection operators. τ_c is the critical resolved shear stress and R^{α} is the transgranular hardening stress due to plastic work. μ_f may be viewed as the frictional coefficient. v_F depicts the roughness degree of the weakness plane. $H(\cdot)$ is the Heaviside step function, which possesses the properties: $H(x) = 1$ if $x \geqslant 0$, otherwise $H(x) = 0$. It is necessary to point out that, for computational convenience, the forward and the reverse slidings are explicitly considered by introducing a twin system for each physical slip system. Otherwise, the first items of (12) and (13) should be replaced by $|\underline{\underline{\sigma}} : \underline{\underline{P}}^{\alpha}|$. Accordingly, the number of slip systems is doubled. The twelve out of twenty-four slip systems are listed in Table 1, while the rest satisfy:

$$\big\{n^{\alpha+12}, s^{\alpha+12}\big\} \equiv \big\{n^{\alpha}, -s^{\alpha}\big\} \tag{14}$$

At mesoscopic level, the viscoplastic strain rate $\underline{\underline{\dot{\varepsilon}}}^{\mathrm{vp}}$ is the summation of contributions from all slip systems:

$$\underline{\underline{\dot{\varepsilon}}}^{\mathrm{vp}} = \sum_{\alpha=1}^{m} \dot{\lambda}^{\alpha} \frac{\partial F^{\alpha}}{\partial \underline{\underline{\sigma}}} = \sum_{\alpha=1}^{m} \dot{\lambda}^{\alpha} \underline{\underline{P}}^{\alpha} + \sum_{\alpha=1}^{m} \dot{\lambda}^{\alpha} v_F H\big(-\sigma_n^{\alpha}\big)\underline{\underline{N}}^{\alpha} \tag{15}$$

In the framework of viscoplasticity, $\dot{\lambda}^{\alpha}$ is the so-called 'pseudo-multiplier', which is explicitly defined as a function of $\underline{\underline{\sigma}}$ and R^{α}. A modified power-type law is introduced [10]:

$$\dot{\lambda}^{\alpha}\big(\underline{\underline{\sigma}}, R^{\alpha}\big) = \begin{cases} \frac{1}{\eta}\big[\big(\frac{f^{\alpha}}{\tau_c^{\alpha} + R^{\alpha}} + 1\big)^{\frac{1}{p}} - 1\big] & \text{if } f^{\alpha} > 0 \\ 0 & \text{if } f^{\alpha} \leq 0 \end{cases} \tag{16}$$

η and p are two strictly positive constants describing the local viscous effect.

To complete the constitutive relations, an integrated form of R^{α} taking into account the cross influence of hardening is given:

$$R^{\alpha} = Q \sum_{\beta=1}^{m} h_{\alpha\beta}\big(1 - \exp\big(-b\lambda^{\beta}\big)\big) \tag{17}$$

Q and b characterize the non-linearity of local hardening (the saturated value and the rate at which saturation is achieved). $h_{\alpha\beta}$ is the interaction matrix allowing the cross influence of the βth slip system on the hardening of the αth slip system. In this paper, the Taylor isotropic hardening model is adopted [11].

The numerical integration for multisurface viscoplasticity is not that direct. The reasons are as follows. Firstly, in stress space, the yield criterion of each slip system (12) can be represented as a surface in a six-dimensional hyperspace. The inner envelopes of these surfaces (24 surfaces) form a non-smooth convex elastic domain. Secondly, the Heaviside step functions in (12) and (13) force us to take into account the state of normal stress, which further aggravate the numerical oscillation.
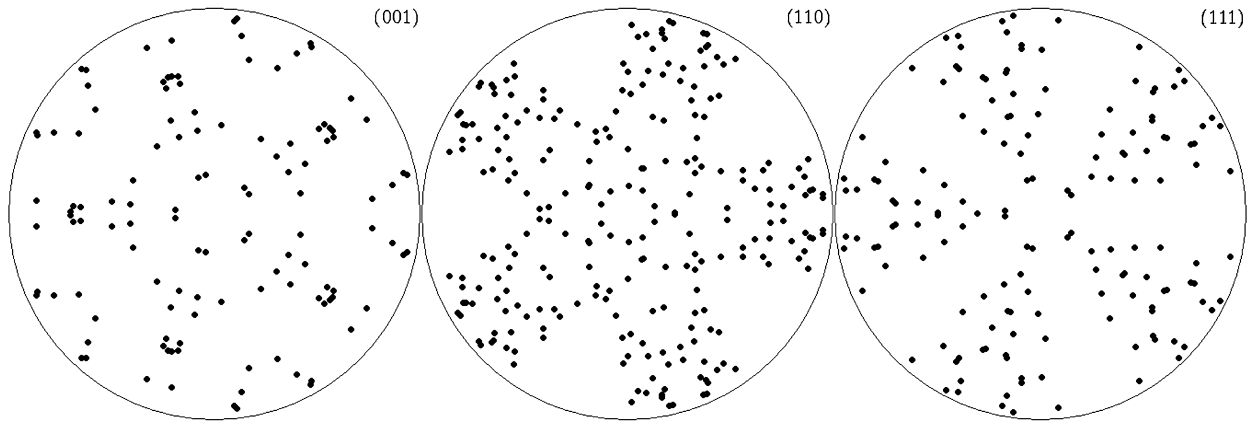
Fig. 2. [0 0 1], [1 1 0] and [1 1 1] pole figures corresponding to forty crystal orientations.

Table 2
Typical values of parameters for an uniaxial tensile test.

E (MPa)	ν	μ_f	ν_f	p	η (s)	τ_c (MPa)
1×10^4	$\frac{1}{3}$	0	0	5×10^{-3}	5×10^{-4}	10

Those problems could be solved by an extended elastic predictor-plastic corrector approach. The difficulty lies in the determination of the actually active slip systems when the stress state happens to locate at certain convexity. A feasible combination of the actually active slip systems is determined by means of two nested iterative procedures. The detailed numerical treatments can be found in [12].

4. Numerical verifications

Several numerical case studies are carried out firstly to check the stability of the proposed elasto-viscoplastic polycrystalline model. Taking into account the macroscopic symmetry, forty crystal orientations are selected to represent the polycrystalline sample [13]. The pole figures of those orientations are given in Fig. 2.

Certain loading history contains more than one steps. Unless otherwise specified, each step is divided into 1000 equal increments. Compressive stress and strain are denoted by negative values. E_{33} is the axial strain coinciding with the axis of the cylindrical sample. $E_{11} = E_{22}$ are the lateral strains and $E_v = E_{33} + 2E_{11}$ is the volumetric strain.

4.1. Taylor factor—the limit of elasto-plastic model

For the polycrystal composed of the perfectly plastic single crystals subjected to uniaxial tension (or compression), the macroscopic stress–strain relation asymptotically approaches a limit—the Taylor factor. The developed elasto-viscoplastic model is now used to verify that limit since the elasto-plastic model will be recovered as long as $\eta \to 0$ (no viscosity) or $p \to 0$ (no rate-sensitivity). We refer to the values proposed by Miehe [12], which are listed in Table 2.

The total strain $E_{33} = 5\%$ is applied with different loading rates: $\dot{E}_{33} = 1 \times 10^{-2}$ s^{-1}, $\dot{E}_{33} = 1 \times 10^{-4}$ s^{-1} and $\dot{E}_{33} = 1 \times 10^{-6}$ s^{-1}. The macroscopic stress Σ_{33} are 28.3052 MPa, 28.2574 MPa and 28.2564 MPa, respectively. These results are obtained in 2000 equal increments. We find that small differences exist among macroscopic stress–strain responses. Therefore, to reproduce the rate-independent response with the rate-dependent model, special attention should be paid to p and η.

Only the stress–strain response with the strain rate $\dot{E}_{33} = 1 \times 10^{-6}$ s^{-1} is given in Fig. 3. Note that the axial stress Σ_{33} has been normalized by σ_y ($\sigma_y = 2\tau_c$). The saturated value 1.412 is close to 1.41, which is a value provided by a rate-independent self-consistent model [14]. Moreover, it does not exceed the variational self-consistent estimation 1.474 [15].

A tentative case study is also carried out—the simple shear test. The total strain $E_{12} = 5\%$ is applied by 5000 equal increments and at the rate of $\dot{E}_{12} = 1 \times 10^{-6}$ s^{-1}. The result is given in Fig. 4. Note that the macroscopic shear stress is normalized by τ_c. To the author's knowledge, for a simple shear test with a self-consistent model, few results are available. The sole result is given by Kröner, Budiansky and Wu (KBW) in their model, and the saturated value is 1.658. The value predicted by our model is 1.578, which is much softer and seems reasonable.

The results titled as KBW in Fig. 3 and Fig. 4 are reproduced by our model. The only thing we need to do is to replace $\mathbb{L}$ by $\mathbb{C}$ in all derivations.
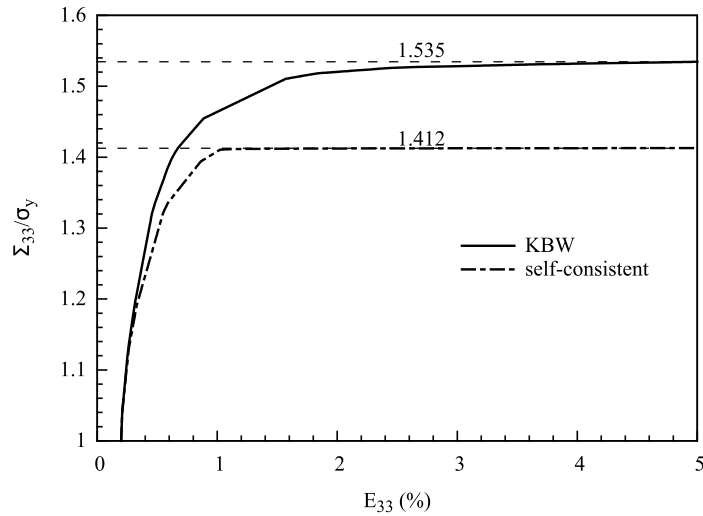
Fig. 3. Taylor factor reproduced by the self-consistent rate-dependent model with an axial stress normalized by $\sigma_y = 2\tau_c$.
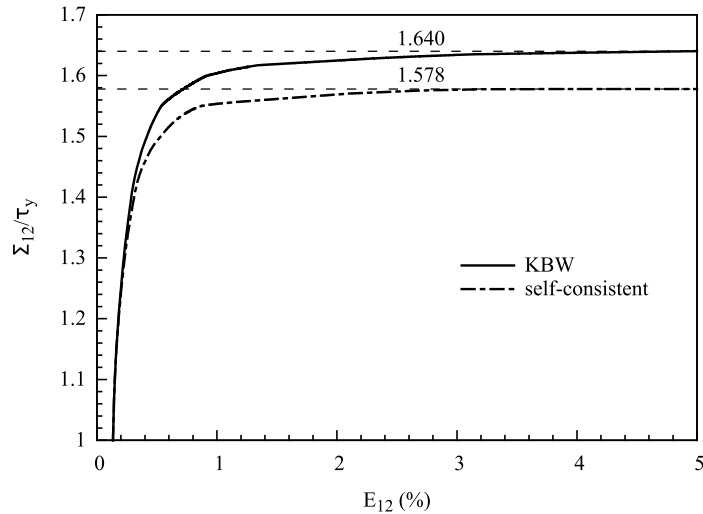
Fig. 4. Taylor factor reproduced by the self-consistent rate-dependent model with a shear stress normalized by τ_c.

4.2. Parametric studies

The influences of parameters η and p on stress–strain response are studied. The parameters are listed in Table 2, except the initial critical stress $\tau_c = 20$ MPa and the parameters concerning the isotropic hardening: $h_{\alpha\beta} = 1$, $b = 100$, and $Q = 20$ MPa.

The total axial strain $E_{33} = 5\%$ is applied at the rate of 1×10^{-2} s^{-1}. The results are given in Fig. 5 and Fig. 6. It is worth noting that the larger η and p, the higher stress responses we obtain. In fact, (16) essentially indicates that as η and p increase, the viscoplastic strain decreases.

Fig. 7 and Fig. 8 show effects of η and p on long-term viscoplastic strain. The whole process is divided into two steps. Firstly, the polycrystal is loaded to 100 MPa at the rate of 2.5×10^{-2} MPa $\cdot$ s^{-1}. Secondly, the polycrystal is left under the action of constant stress for 24 h. Only the results in the second step are presented. Attention should be paid to the opposite results as the viscoplastic strains decrease with the increase of η and p, which means that parameters η and p play completely different roles during the short-term (loading stage) and the long-term (no loading stage) situations.

Fig. 9 shows another important rate-dependent relaxation behavior, which is obtained by firstly prescribing the uniaxial strain $E_{33} = 1\%$ at the rate of 1×10^{-6} s^{-1} and then maintaining this strain for 24 h.
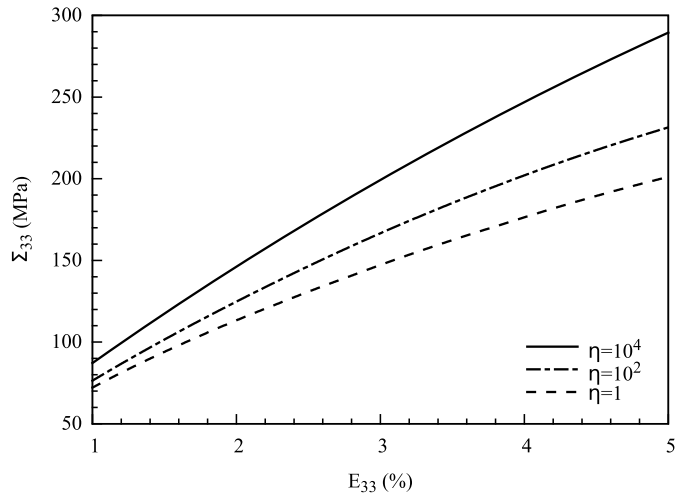
Fig. 5. Influence of parameter η with the fixed value $p = 0.1$.
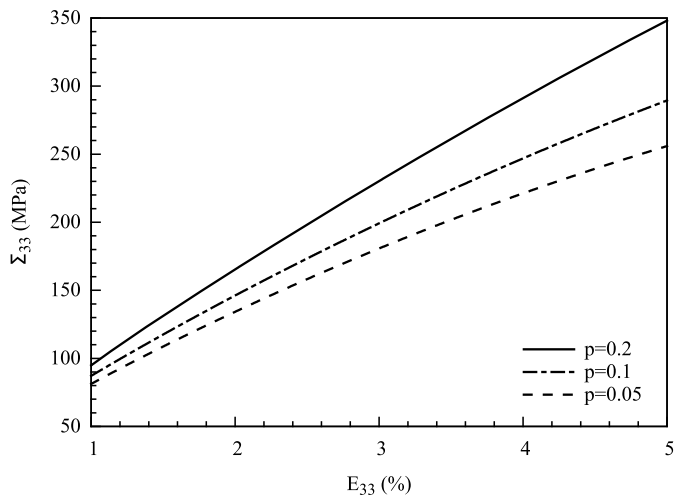
Fig. 6. Influence of parameter p with the fixed value $\eta = 10^4$ s.
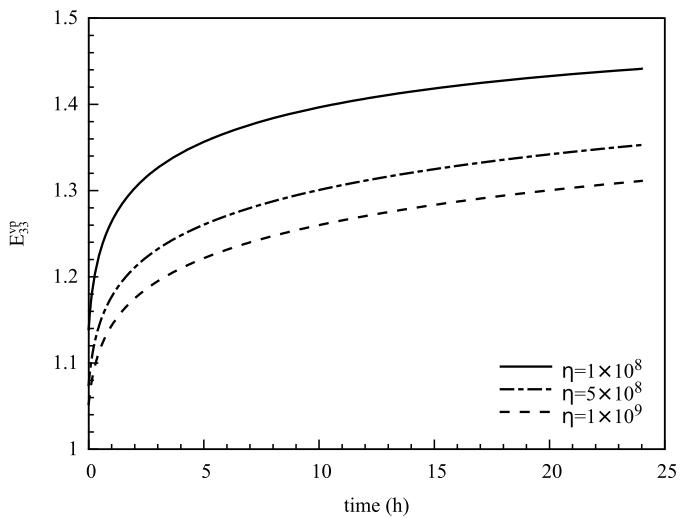
Fig. 7. Long-term influence of parameter η with the fixed value $p = 0.1$.
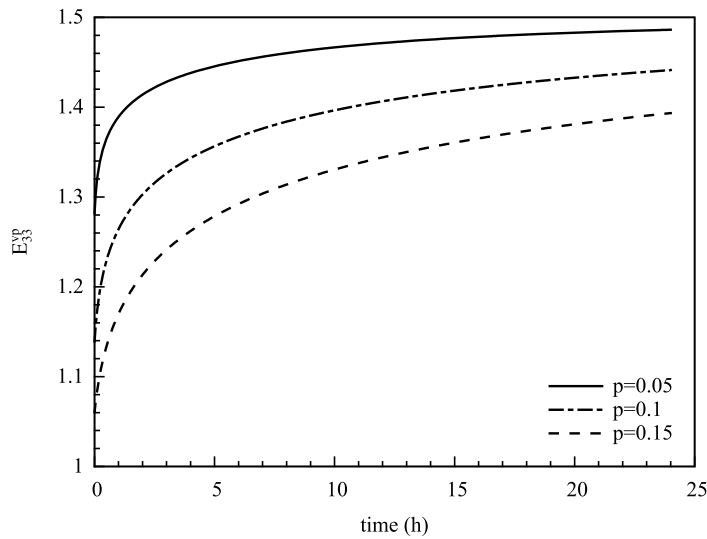
Fig. 8. Long-term influence of parameter p with the fixed value $\eta = 10^8$ s.
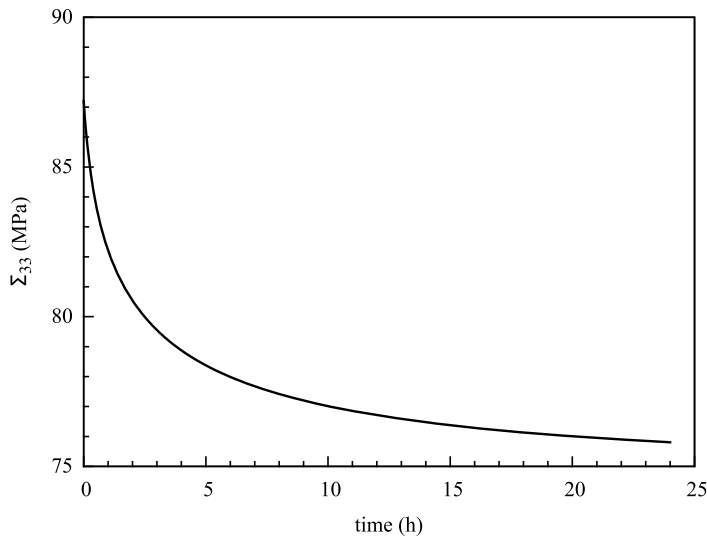
Fig. 9. Relaxation test with fixed values $p = 0.1$ and $\eta = 10^8$ s.

5. Laboratory tests verification

Now, the developed elasto-viscoplastic polycrystalline model will be applied to reproduce both short- and long-term behaviors of a typical granite (Lac du Bonnet), which has been widely studied at the Underground Research Laboratory (URL) in Canada for feasibility studies of nuclear waste storage [16]. Detailed information about the experiments can be found in [17].

5.1. Short-term behavior

The model parameters should be identified at first before reproducing the laboratory tests. In total, nine parameters are necessary to characterize the response of an individual grain. η and p are identified from an uniaxial time-dependent test in dry conditions, while the rest of the parameters are identified by performing calibration on a triaxial compression test, as Fig. 10 shows. Detailed processes are explained in [18]. The typical parameters used for reproduction are given in Table 3.

It is necessary to point out that when the calibrated parameters are used to reproduce the short-term behavior, the parameters p and η could not be the same as those used in a long-term behavior simulation. Here, we proposed an alternative approach. Instead of adjusting p and η simultaneously, we seek to obtain the same affect by modifying the loading rate. The corresponding loading rate is firstly identified from a triaxial test, as Fig. 10 shows. Then the other two
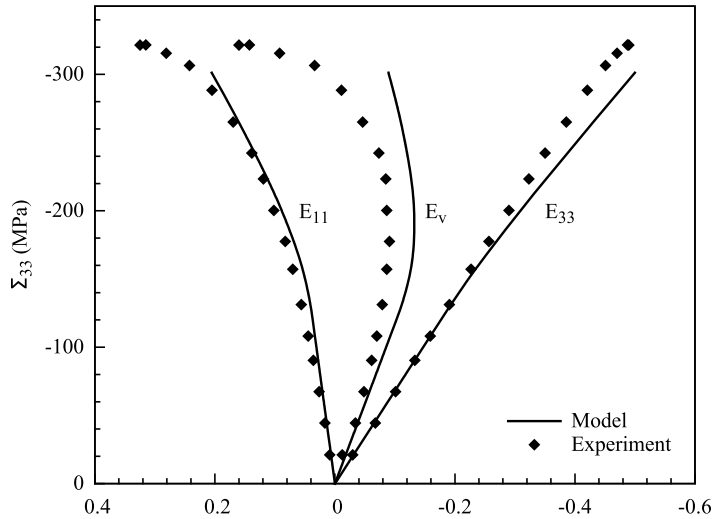
Fig. 10. Comparison between experimental data and model predictions−triaxial compression with confining pressure −10 MPa.

Table 3
Typical values of parameters for the time-dependent behavior.

E (MPa)	ν	μ_f	v_f	η (s)	p	τ_c (MPa)	$h_{\alpha\beta}$	b	Q (MPa)
6.8×10^4	0.21	0.4	0.6	1×10^9	0.9	35	1.0	100	40
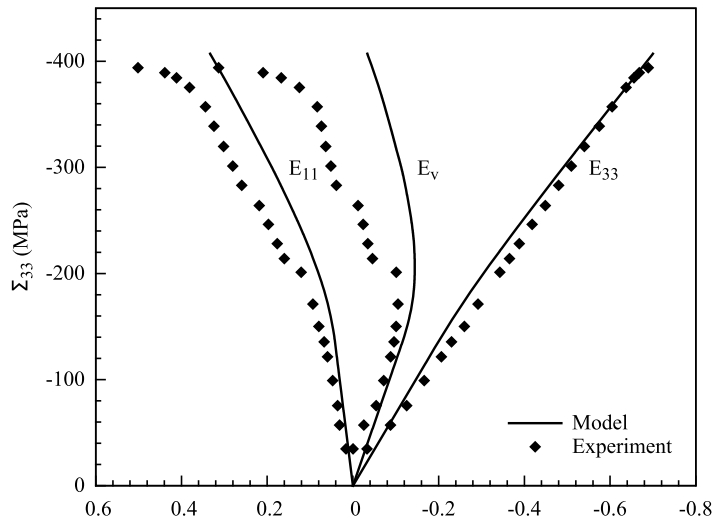
Fig. 11. Comparison between experimental data and model predictions−triaxial compression with confining pressure −20 MPa.

tests are simulated with the same loading rate. The results in Fig. 11 and Fig. 12 show that there is a good correlation between the model's predictions and experimental data.

5.2. Long-term behavior

The long-term responses of granite are depicted in dry and wet conditions. Due to the insufficiency of experiment data, the simulations are qualitative rather than quantitative. The parameters are the same as those used in short-term behavior simulations, except for the wet case. The change of the environment conditions is simply considered by reducing the initial and the peak stress. For the wet condition, $\tau_c = 29$ MPa and $Q = 6$ MPa.

The comparisons between the model's predictions and experimental data are given in Figs. 13 and 14. The trends of lateral strain in dry and wet conditions are obtained by keeping the specimen strained under $\Sigma_{33} = -143$ MPa for 70 days and $\Sigma_{33} = -137$ MPa for 80 days, respectively. Fig. 14 clearly shows the important role of water. Although the load in wet condition is lower than that in dry condition, the rate and the amount of deformation are much larger.
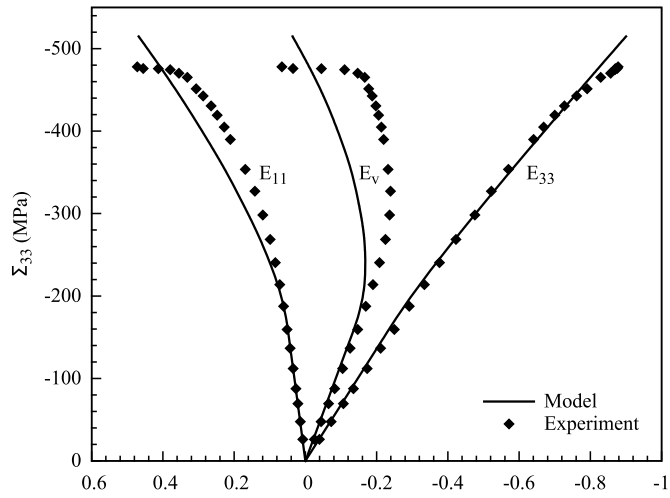
Fig. 12. Comparison between experimental data and model predictions–triaxial compression with confining pressure −40 MPa.
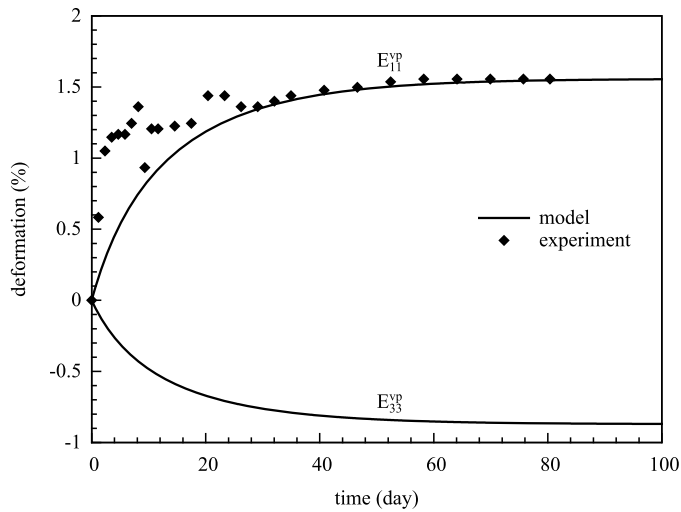
Fig. 13. Comparison between experimental data and model predictions–uniaxial creep test in dry condition.
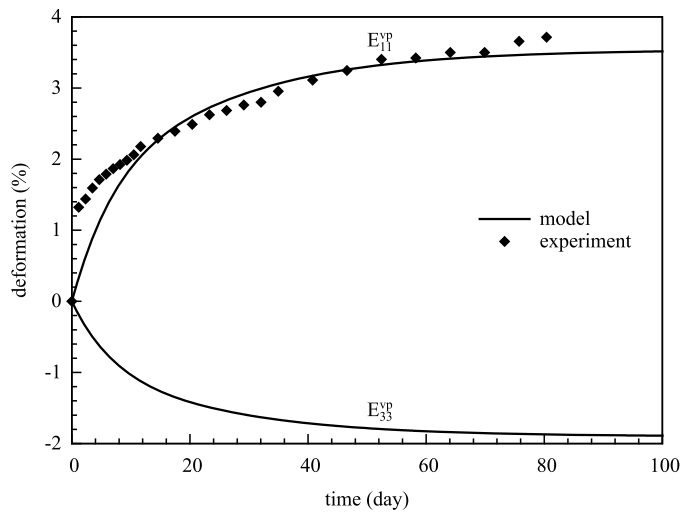
Fig. 14. Comparison between experimental data and model predictions–uniaxial creep test in wet condition.

6. Conclusion

A micromechanical constitutive model based on the self-consistent scheme is proposed to describe the time-dependent behavior of granite. The limitation of Hill's incremental formulations is circumvented by modifying the form of the macroscopic constitutive relation and introducing a consistent algorithmic tangent operator. The characteristics of pressure sensitivity and dilation due to plastic flow are described by introducing a Mohr–Coulomb type yield criterion and a non-associated plastic potential. The performance of the developed model is checked not only by reproducing the Taylor factor and various macroscopic phenomenological aspects, but also by the comparisons between numerical predictions and experimental data. The future work is going to include the effect of the interface, which is essential to describe the material's post-peak stress–strain response.

Acknowledgements

Appendix A. Consistent algorithmic tangent moduli

Differentiating the stress–strain relation (10) and the viscoplastic flow rule (15) at the equilibrium state $t = t_{k+1}$:

$$\mathrm{d}\underline{\underline{\sigma}}_{k+1} = \mathbb{C} : \left(\mathrm{d}\underline{\underline{\varepsilon}}_{k+1} - \mathrm{d}\underline{\underline{\varepsilon}}^{\mathrm{vp}}_{k+1} \right) \tag{18}$$

$$\mathrm{d}\underline{\underline{\varepsilon}}^{\mathrm{vp}}_{k+1} = \sum_\alpha \mathrm{d}\Delta\lambda^\alpha_{k+1}\underline{\underline{M}}^{F,\alpha}_{k+1} \quad \alpha \in J_{k+1} \tag{19}$$

where

$$\underline{\underline{M}}^{F,\alpha}_{k+1} = \underline{P}^\alpha + v_{\mathrm{F}} H\left(-\sigma^\alpha_{n,k+1}\right)\underline{N}^\alpha$$

J_{k+1} is the set composed of actually active slip systems.

Applying an implicit backward Euler method to (16) and then differentiating it yields:

$$\underline{\underline{M}}^{f,\beta}_{k+1} : \mathrm{d}\underline{\underline{\sigma}}_{k+1} - \sum_\alpha \left[E^{\beta\alpha}_{k+1}\right]\mathrm{d}\Delta\lambda^\alpha_{k+1} = 0 \quad \alpha, \beta \in J_{k+1} \tag{20}$$

where

$$\underline{\underline{M}}^{f,\beta}_{k+1} = \underline{P}^\beta + u_{\mathrm{f}} H\left(-\sigma^\beta_{n,k+1}\right)\underline{N}^\beta$$

$$E^{\beta\alpha}_{k+1} = h_{\beta\alpha} b Q \exp\left(-b\lambda^\alpha_{k+1}\right)\left(1 + \frac{\Delta\lambda^\beta_{k+1}\eta}{\Delta t}\right)^p + \delta_{\beta\alpha}\frac{p\eta(\tau_{\mathrm{c}} + R^\beta_{k+1})}{\Delta t}\left(1 + \frac{\Delta\lambda^\beta_{k+1}\eta}{\Delta t}\right)^{p-1}$$

Combining (18), (19) and (20), we obtain:

$$\mathrm{d}\Delta\lambda^\alpha_{k+1} = \sum_\beta \left[g^{\alpha\beta}_{k+1}\right]\underline{\underline{M}}^{f,\beta}_{k+1} : \mathbb{C} : \mathrm{d}\underline{\underline{\varepsilon}}_{k+1} \quad \beta \in J_{k+1} \tag{21}$$

with

$$G^{\beta\alpha}_{k+1} = \underline{\underline{M}}^{f,\beta}_{k+1} : \mathbb{C} : \underline{\underline{M}}^{F,\alpha}_{k+1} + E^{\beta\alpha}_{k+1} \quad \text{and} \quad [g] = [G]^{-1}$$

Finally, combining (18), (19) and (21) yields the expression for the consistent algorithmic tangent moduli:

$$\mathbb{L}^{\mathrm{alg}} = \frac{\mathrm{d}\underline{\underline{\sigma}}_{k+1}}{\mathrm{d}\underline{\underline{\varepsilon}}_{k+1}} = \mathbb{C} - \sum_\alpha \sum_\beta \left[g^{\alpha\beta}_{k+1}\right]\left(\mathbb{C} : \underline{\underline{M}}^{F,\alpha}_{k+1}\right) \otimes \left(\underline{\underline{M}}^{f,\beta}_{k+1} : \mathbb{C}\right) \quad \alpha, \beta \in J_{k+1} \tag{22}$$

If $J_{k+1} = \emptyset$, $\mathbb{L}^{\mathrm{alg}} = \mathbb{C}$.

References

[1] J.F. Shao, K.T. Chau, X.T. Feng, Modeling of anisotropic damage and creep deformation in brittle rocks, Int. J. Rock Mech. Min. Sci. 43 (2006) 582–592.

[2] Q.Z. Zhu, D. Kondo, J.F. Shao, V. Pensée, Micromechanical modelling of anisotropic damage in brittle rocks and application, Int. J. Rock Mech. Min. Sci. 45 (2008) 467–477.

[3] Q.Z. Zhu, J.F. Shao, D. Kondo, A micromechanics-based elastoplastic damage model for granular materials at low confining pressure, Int. J. Plast. 26 (2010) 586–602.

[4] U.F. Kocks, C.N. Tomé, H.R. Wenk, Texture and Anisotropy: Preferred Orientations in Polycrystals and Their Effect on Materials Properties, Cambridge University Press, Cambridge, UK, 2000.

[5] A. Molinari, G. Canova, S. Ahzi, A self-consistent approach of the large deformation polycrystal viscoplasticity, Acta Metall. 35 (1987) 2983–2994.

[6] R.A. Lebensohn, C.N. Tomé, A self-consistent anisotropic approach for the simulation of plastic deformation and texture development of polycrystals, Acta Metall. Mater. 41 (1993) 2611–2624.

[7] R. Soulié, S. Mérillou, O. Terraz, D. Ghazanfarpour, Modeling and rendering of heterogeneous granular materials: granite application, Comput. Graph. Forum 26 (2007) 66–79.

[8] A.V. Hershey, The elasticity of an isotropic aggregate of anisotropic cubic crystals, J. Appl. Mech. 21 (1954) 236–240.

[9] R. Hill, Continuum micro-mechanics of elastoplastic polycrystals, J. Mech. Phys. Solids 13 (1965) 89–101.

[10] D. Peric, D.R.J. Owen, A model for finite strain elasto-plasticity based on logarithmic strains: computational issues, Comput. Methods Appl. Mech. Eng. 94 (1992) 35–61.

[11] G.I. Taylor, Plastic strain in metals, J. Inst. Met. 62 (1938) 307–324.

[12] C. Miehe, J. Schröder, A comparative study of stress update algorithms for rate-independent and rate-dependent crystal plasticity, Int. J. Numer. Methods Eng. 50 (2001) 273–298.

[13] P. Pilvin, Approches multi-échelles pour la prévision du comportement anélastique des métaux, Ph.D. thesis, Université Pierre et Marie Curie, 1990.

[14] K. Yoshida, R. Brenner, B. Bacroix, S. Bouvier, Effect of regularization of Schmid law on self-consistent estimates for rate-independent plasticity of polycrystals, Eur. J. Mech. A, Solids 28 (2009) 905–915.

[15] M.V. Nebozhyn, P. Gilormini, P.P. Castaneda, Variational self-consistent estimates for cubic viscoplastic polycrystals: the effects of grain anisotropy and shape, J. Mech. Phys. Solids 49 (2001) 313–340.

[16] J.F. Shao, D. Hoxha, M. Bart, F. Homand, G. Duveau, M. Souley, N. Hoteit, Modelling of induced anisotropic damage in granites, Int. J. Rock Mech. Min. Sci. 36 (1999) 1001–1012.

[17] C.D. Martin, R.S. Read, J.B. Martino, Observations of brittle failure around a circular test tunnel, Int. J. Rock Mech. Min. Sci. 34 (1997) 1065–1073.

[18] T. Zeng, J.F. Shao, W.Y. Xu, Multiscale modeling of cohesive geomaterials with a polycrystalline approach, Mech. Mater. 69 (2014) 132–145.